BRITTLE-DUCTILE TRANSITION IN POROUS ROCKS BY CAP MODEL

By Vlado A. Lubarda,[1] Sreten Mastilovic,[2] and Jaroslaw Knap[3]

ABSTRACT: A pressure-dependent cap model that is capable of describing the brittle-ductile transition in porous rocks is proposed. The model consists of a hardening Drucker-Prager yield cone with a nonassociative flow rule, an ellipsoidal cap with an associative flow rule, and a failure or limiting surface. This surface designates the stress states at the inception of failure below brittle-ductile transition, or the onset of ideally plastic response above brittle-ductile transition. The appropriately combined structures of the associative and nonassociative flow rules eliminate the difficulties associated with a singular corner region at the intersection of the cap and failure surface. A cross hardening between the cap and cone is discussed. The model is capable of a good qualitative agreement with experimental data, as demonstrated by the results of the triaxial compression tests under various amounts of the confining pressure. A stress-strain response with inelastic volume dilatancy at lower confinements, and an increased ductility and hardening rates at higher confinements, are well predicted.

INTRODUCTION

Except in low-porosity crystalline rocks at high temperatures, where the crystal plasticity mechanisms operate, in most other cases the inelastic deformation in rocks is a consequence of the nucleation and propagation of microcracks originated at the surface of pores or other inhomogeneities within a rock sample, such as inclusions and grain boundaries. The nucleation and growth of microcracks under overall compressive loads can, for example, occur due to tensile stress concentrations at the perimeter of microvoids, bending of the long beam-like grains, or Hertzian contact stresses between the cement and grains. In low porosity, compact rocks frictional sliding of crack surfaces may destabilize existing shear cracks, causing them to kink and develop wing cracks.

The response of a compressed brittle rock strongly depends on the lateral or confining pressure. In stress-controlled tests at low confinement the mode of failure is brittle. The onset of failure is sudden and is not preceded by significant inelastic strains. An unconfined specimen fails by axial splitting or slabbing along one or few contiguous failure planes (Sammis and Ashby 1986; Horii and Nemat-Nasser 1986; Ashby and Sammis 1990). The failure planes form by unstable growth of major cracks created through interaction and coalescence of the preexisting and nucleated microcracks. The stress-strain curve has a short nonlinear range corresponding to small deformability of the sample before its splitting fracture. More important and complex is the behavior of rocks in confined conditions, which are in crustal conditions provided by existing displacement constraints. When a rock specimen is compressed under applied confinement, axial splitting is suppressed, and up to a certain level of the confining pressure specimen fails in a narrow region of high concentration interacting microcracks. This localized region is usually referred to as a shear band or fault, whose inclination to the longitudinal compression axis depends on the amount of applied confinement. Sometimes, a localization into a few shear bands become apparent. The nonlinear range of the stress-strain curve and deformability of the sample before this type of failure are more pronounced, and they increase with the increase of the confining pressure. The localization studies with pressure dependent constitutive models, such as those of Rudnicki and Rice (1975), indicate that in confined triaxial compression the shear band, beyond which a macroscopically nonhomogeneous deformation develops, occurs corresponding to a point on the descending (softening) portion of the stress-strain curve. Zheng et al. (1991) experimentally found that in limestone under sufficient confinement the microcracks were rather uniformly distributed over the entire specimen, even in the post-peak regime of the stress-strain response.

At high levels of lateral confinement, the formation of a shear band is suppressed and homogeneous microcracking (cataclastic flow) prevails throughout the sample. Although, this involves microscopically brittle processes, the macroscopic result is a quasi- or pseudoductile overall response, with a raising stress-strain curve up to high levels of compressive strain, akin to hardening in ductile metals. In porous rocks this macroscopic ductility reflects distributed grain-scale crushing and microcracking (Wong 1990). The microcrack density increases and the microcrack lengths decrease with the increase of the confining pressure. With some rocks such as porous quartzite, however, the cataclastic flow is only a transient behavior, since deformation becomes localized at strains greater than about 25%.

The change of the deformation mode that occurs at a certain value of the confining pressure, at which the formation of shear band and strain softening are suppressed, is referred to in rock mechanics as the brittle-ductile transition (Jaeger and Cook 1976; Paterson 1978; Kranz 1983; Read and Hegemier 1984; Hegemeier and Read 1985; Zhang et al. 1989; Wong et al. 1992). Available micromechanical and phenomenological models of the brittle-ductile transition are still very limited. This is not surprising since the onset of brittle-ductile transition depends on a complicated phenomenon of the microcrack interaction, stabilization of microcracking by applied confining pressure, rock composition, temperature, strain rates, etc. Also, the value of the confining pressure at which the transition occurs is often difficult to determine experimentally, since it may be sensitive to the loading and test boundary conditions.

A micromechanical model based on fracture mechanics was constructed by Sammis and Ashby (1986) to analyze the effects of pressure and porosity on the inelastic response of porous rocks. Horii and Nemat-Nasser (1986) examined the micromechanics of axial splitting, faulting, and brittle-ductile transition using available experimental results and suggested mathematical models. The effects of pressure and porosity on the micromechanics of the brittle-ductile transition in quartzite has been studied by Hirth and Tullis (1989). Fredrich et al. (1989) used the samples of Carrara marble at room temperature and under confining pressures spanning the range in me-

[1]Visiting Assoc. Prof., Dept. of Mech. and Aerosp. Engrg., Arizona State Univ., Tempe, AZ 85287-6106.

[2]Grad. Student, Dept. of Mech. and Aerosp. Engrg., Arizona State Univ., Tempe, AZ.

[3]Grad. Student, Dept. of Mech. and Aerosp. Engrg., Arizona State Univ., Tempe, AZ.

Note. Associate Editor: Robert Y. Liang. Discussion open until December 1, 1996. To extend the closing date one month, a written request must be filed with the ASCE Manager of Journals. The manuscript for this paper was submitted for review and possible publication on March 16, 1995. This paper is part of the ***Journal of Engineering Mechanics***, Vol. 122, No. 7, July, 1996. ©ASCE, ISSN 0733-9399/96/0007-0633–0642/$4.00 + $.50 per page. Paper No. 10279.

chanical behavior from brittle to ductile, and discussed some theoretical treatments of failure based on the bifurcation analysis and fracture mechanics. Wong (1990) used acoustic emission measurements to study pressure-induced grain crushing and the brittle-ductile transition in porous sandstones. Brittle-ductile transition in rocks was also studied by Zhang et al. (1989), Evans et al. (1990), Rutter and Hadizadeh (1991), and others.

In the present paper the brittle-ductile transition is approached from the phenomenological point of view by using an adequate pressure-dependent cap model. Previously, pressure-dependent constitutive models were extensively used to describe many features of inelastic response of geomaterials. The model based on the Mohr-Coulomb failure criterion assumes that failure is governed by a maximum shear stress, whose critical value depends on the cohesion of the material, the normal stress on the plane of maximum shear stress, and the angle of internal friction. As such, this criterion is a pressure-dependent generalization of the Tresca criterion. The Drucker-Prager (Drucker and Prager 1952) criterion is a generalization of the Mises criterion. The yielding occurs when the mean value of all shearing stresses reaches a critical value that linearly depends on the hydrostatic stress. A modified Drucker-Prager criterion with a nonlinear (parabolic or exponential) dependence on the hydrostatic stress was also used, e.g., Bresler and Pister (1958), DiMaggio and Sandler (1971), and Simo et al. (1988). More involved representations of the pressure-dependent yield condition, including the third stress invariant, have been promoted in studying soils, sands, rocks, and concretes, as evidenced by the work of Lade and Duncan (1975), Lade (1977), Kim and Lade (1984), Desai (1980), Han and Chen (1985), Frantziskonis et al. (1986), Desai and Varadarajan (1987), Chen and Han (1988), among others. Such modifications change the shape of the yield surface in stress space or its subspaces, such as the deviatoric plane. However, the yield or failure conditions are still expressed as the scalar functions of three stress invariants. Hence, inelastic response is assumed to be isotropic, independent of the principal stress directions and their changes. Consequently, the models are more suitable to proportional or near proportional loadings. Furthermore, in materials such as rocks, they are more appropriate if sufficient confinement is provided, because microcracking or other microfailures then tend to be more isotropically distributed.

For some geomaterials above a certain amount of confinement, the pressure-dependent models of the Drucker-Prager or a similar type overestimate the yield stress, and inadequately predict the volumetric strain response. Folowing an original idea by Drucker et al. (1957), DiMaggio and Sandler (1971) developed a cap model by closing the yield cone (or pyramid) in principal stress space with a cap that crosses the hydrostatic stress axis. This modification, therefore, allows compressive strain-rates and yield under hydrostatic pressure. Both, physical and numerical aspects of the implementation of the pressure-dependent cap model were subsequently studied by many authors, e.g., Prevost and Höeg (1975), Sandler et al. (1976), Lade (1977), Sandler and Rubin (1979), Bathe et al. (1980), Zaman et al. (1982), Desai and Siriwardane (1984), Resende and Martin (1985), and Simo et al. (1988). An elliptically shaped cap was most commonly used, although spherical, parabolic, and plane caps were considered as well. The conical part of the yield surface is usually assumed to be fixed in stress space, corresponding to ideally plastic material response, while the cap moves as prescribed by a hardening of the material during its porosity reduction and volumetric compaction. To define this hardening, a relationship between pressure and volume change under pure compressive loading needs to be known. This issue by itself received a significant attention from both experimental and theoretical point of view, as recently discussed for porous rocks by Zhang et al. (1990).

It is known and has been experimentally observed that for many geomaterials the associative flow rules do not accurately predict some essential features of the mechanical response. For example, they tend to overestimate the inelastic volume changes in geomaterials like rocks and soils. Consequently, the nonassociative flow rules have been employed for such materials, e.g., Rudnicki and Rice (1975), Nemat-Nasser and Shokooh (1980), Nemat-Nasser (1983), Senseny et al. (1983), Chandler (1985), and Desai et al. (1986). The inelastic strain rate is then assumed to be normal to inelastic potential surface, which is distinct from the yield surface. For materials described by the nonassociative flow rules there are at least some cycles of stress and strain that violate Drucker's and Ilyushin's work inequalities, so that neither of the corresponding famous postulates generally apply. It should also be mentioned that previously discussed models mostly apply for loading situations with the overall compressive states of stress. If the loading enters the tensile stress domain, the models are usually extended by introducing some type of a tension cutoff surface, as discussed, for example, by Sandler and Rubin (1979), Resende and Martin (1984), Desai and Varadarajan (1987), and Simo et al. (1988).

To complete the constitutive description, it is furthermore needed to describe the elastic part of the total response. This in general poses significant difficulties because the continuing deformation of brittle materials such as rocks is accompanied by a progressive degradation of elastic macroproperties, and the change of material elastic symmetry. Several analytical models have been suggested to estimate the effective elastic properties of solids weakened by a given distribution of many cracks or other defects. An extensive review of these models can be found in a treatise by Nemat-Nasser and Hori (1993). Recently, fourth-order elastic compliance or stiffness tensors have been often utilized as the appropriate damage tensors, e.g., Ortiz (1985), Simo and Ju (1987), Ju (1989), Yazdani and Schreyer (1989), Lubarda (1994), Lubarda and Krajcinovic (1995a, 1995b), and Lubarda et al. (1995). These papers also address various aspects of the rate-type theory of inelastic deformation associated with progressive fracturing and deterioration of elastic material properties. Earlier research in this direction was done by Dougill (1975, 1983), Dragon and Mróz (1979), Bažant and Kim (1979), and Dougill and Rida (1980). Since the main interest in this paper is a description of the brittle-ductile transition, the attention is focused to overall compressive stress states, with a sufficient amount of confinement so that microfracturing within a representative volume element is approximately uniform and reasonably isotropic. Elastic isotropy of the material can then be assumed to persist, with appropriately modified values of the corresponding elastic constants. This further enables the use of the yield or failure conditions that can be expressed as isotropic functions of the stress tensor, and, therefore, written in terms of the three stress invariants. Otherwise, the inclusion of elastic anisotropy would also require the use of the anisotropic yield and failure conditions, which cannot be expressed only in terms of the stress invariants.

The content of the paper is as follows. A hardening Drucker-Prager yield cone with an adequate nonassociative flow rule is introduced in the second section. The ellipsoidal cap surface that crosses the hydrostatic stress axis and a corresponding associative flow rule are studied in the third section. In the fourth section, the failure or limiting surface is introduced, which designates the inception of actual failure, or the onset of ideally plastic response. The constitutive model is applied in the fifth section to triaxial compression of Salem limestone under various amounts of the confining pressure. Conclusions are given in the final section.

NONASSOCIATIVE FLOW RULE WITH DRUCKER-PRAGER YIELD CRITERION

To describe the pressure-dependent yield of soils, Drucker and Prager (1952) suggested a yield condition

$$f = J_2^{1/2} - \mu I_1 - k, \quad f = 0 \tag{1}$$

where $\mu > 0$ is a material parameter related to angle of internal friction; $I_1 = \sigma_{kk}$ = first stress invariant; $J_2 = (1/2)S_{ij}S_{ij}$ = second invariant of deviatoric stress $S_{ij} = \sigma_{ij} - (1/3)\sigma_{kk}\delta_{ij}$; and k = a parameter related to cohesion of the material, which defines the size of the yield surface. As customary in geo and rock mechanics, compressive stresses and strains are assumed to be positive. The components δ_{ij} are the Kronecker delta components. If the yield stress in uniaxial compression is K, from Fig. 1 it follows that $k = (1 - \sqrt{3}\mu)K$. For $\mu = 0$, the Drucker-Prager condition reduces to the (pressure-independent) von Mises yield condition. In soil mechanics the yielding is usually assumed to be perfectly plastic, hence k is taken to be constant. Having in mind application to rocks, we will assume k to be a function of the monotonically increasing parameter φ, related to a generalized inelastic strain, so that $k = k(\varphi)$. If the parameter μ is also dependent on φ, the corresponding hardening is of a nonuniform kind. As is well known, the associative flow rules can inadequately predict inelastic volume changes in geomaterials like rocks and soils. Consequently, the nonassociative flow rules have been commonly utilized for such materials, with the inelastic potential function $\hat{f}$ different from the yield function. The inelastic part of the deformation rate tensor, here referred to as the inelastic strain rate, is then assumed to be given by

$$D_{ij}^I = \dot{\varphi}\frac{\partial \hat{f}}{\partial \sigma_{ij}} \tag{2}$$

A simple modification of the Drucker-Prager yield function suggested for the potential $\hat{f}$ is

$$\hat{f} = J_2^{1/2} - \Phi(I_1, \varphi) \tag{3}$$

where Φ = an appropriately specified function of its indicated arguments. Substitution of (3) into (2) gives

$$D_{ij}^I = \dot{\varphi}\left(\frac{S_{ij}}{2J_2^{1/2}} - \phi\delta_{ij}\right) \tag{4}$$

where $\phi = \partial\Phi/\partial I_1$. Clearly, the deviatoric and volumetric parts of the inelastic strain rate are, respectively

$$d_{ij}^I = \dot{\varphi}\frac{S_{ij}}{2J_2^{1/2}}; \quad D_{kk}^I = -3\dot{\varphi}\phi \tag{5}$$

The rate of the parameter φ can now be easily related to the rates of the generalized inelastic strains by

$$\dot{\varphi} = (2d_{ij}^I d_{ij}^I)^{1/2} = \frac{1}{(1 + 6\phi^2)^{1/2}}(2D_{ij}^I D_{ij}^I)^{1/2} \tag{6}$$

Physically, the parameter 3ϕ represents a dilatancy factor (Rudnicki and Rice 1975; Nemat-Nasser and Shokooh 1980), since

$$3\phi = -\frac{D_{kk}^I}{(2d_{ij}^I d_{ij}^I)^{1/2}} \tag{7}$$

Recall the adopted convention by which a tensile volumetric strain (dilation) is considered to be negative. If a more general representation of the potential function is assumed, for example, $\hat{f} = \hat{f}(I_1, J_2, \varphi)$, the dilatancy factor becomes $3\phi/(2J_2^{1/2}\partial\hat{f}/\partial J_2)$, which is equal to the right-hand side of (7).

The consistency condition for the continuing inelastic deformation gives the expression for $\dot{\varphi}$ in terms of the objective, Jaumann stress rate $\mathring{\sigma}_{ij}$ as

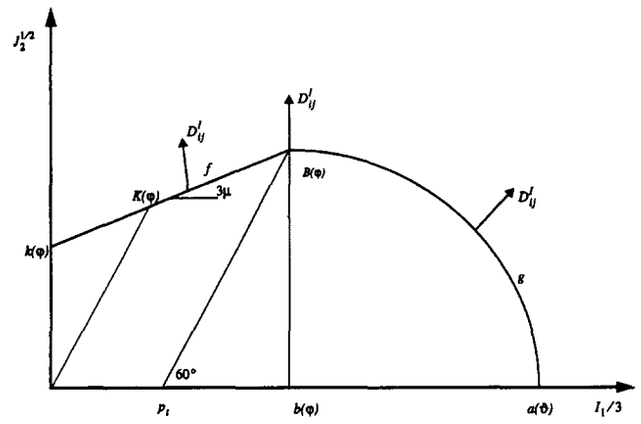

FIG. 1. Yield Surface Consisting of Drucker-Prager Cone *f* and Ellipsoidal Cap *g*

$$\dot{\varphi} = \frac{1}{h}\left(\frac{S_{ij}}{2J_2^{1/2}} - \mu\delta_{ij}\right)\mathring{\sigma}_{ij} \tag{8}$$

where $h = dk/d\varphi$ if μ = a constant; and $h = dk/d\varphi + I_1 d\mu/d\varphi$ if μ depends on φ. Substitution of (8) into (4) provides the final expression for the inelastic strain rate

$$D_{ij}^I = \frac{1}{h}\left(\frac{S_{ij}}{2J_2^{1/2}} - \phi\delta_{ij}\right)\left(\frac{S_{kl}}{2J_2^{1/2}} - \mu\delta_{kl}\right)\mathring{\sigma}_{kl} \tag{9}$$

Most often, ϕ in (9) is assumed to be constant ($\neq \mu$), corresponding to a linear dependence of Φ on the hydrostatic stress (Lubarda et al. 1996). In the subsequent analysis, however, it will be assumed that the function Φ appearing in (3) has a parabolic dependence on the hydrostatic stress, such that

$$\Phi(I_1, \varphi) = B(\varphi) - d_0(\varphi)[b(\varphi) - I_1/3]^n \tag{10}$$

where n = an appropriate exponent. This structure of Φ predicts positive inelastic dilatancy that gradually decreases along the hydrostatic axis, becoming zero at the brittle-ductile transition pressure. The experiemental data for Salem limestone (Green 1992) indicate that inelastic volume changes tend to disappear at the brittle-ductile transition. The function $B(\varphi)$ can be experimentally determined from the triaxial compression test under the confining pressure p_t, at which the brittle-ductile transition occurs. In this test $B = \sigma/\sqrt{3}$, where σ = stress difference in the considered triaxial compression test. From Fig. 1, the parameter $b(\varphi)$, which represents the hydrostatic stress corresponding to the B value of $J_2^{1/2}$, is related to $B(\varphi)$ by

$$b(\varphi) = p_t + \frac{1}{\sqrt{3}}B(\varphi) \tag{11}$$

The function $d_0(\varphi)$ is introduced to improve fitting of the experimental data. The dilatancy factor corresponding to (10) is

$$3\phi = 3\frac{\partial\Phi}{\partial I_1} = nd_0[b(\varphi) - I_1/3]^{n-1} \tag{12}$$

This becomes zero along the brittle-ductile transition line $I_1/3 = b$, indicating the absence of inelastic volume change during the brittle-ductile transition. Since there is no inelastic volume change during the brittle-ductile transition, B is a function of the generalized inelastic deviatoric strain only, $B = B(\varphi)$. From the geometry in Fig. 1 it follows that $k = (1 - \sqrt{3}\mu)B - 3\mu p_t$, which requires that k also depends on φ only, and not on the inelastic volume change associated with the loading on the Drucker-Prager yield cone. Finally, the function d_0 can be determined from the experimental data of the uniaxial compression test with zero confinement. If $3\phi_0$ denotes the cor-

responding measured dilatancy factor and if μ is assumed to be constant, it readily follows that

$$d_0 = \frac{1}{n}\left(\frac{1-\sqrt{3}\mu}{p_t}\right)^{n-1} 3\phi_0 \tag{13}$$

Loading along Brittle-Ductile Transition

During inelastic loading along the brittle-ductile transition line $I_1 = 3b(\varphi)$, there is no inelastic dilation ($\phi = 0$), and (9) reduces to

$$D^I_{ij} = \frac{1}{h}\frac{S_{ij}}{2J_2^{1/2}}\left(\frac{S_{kl}}{2J_2^{1/2}} - \mu\delta_{kl}\right)\dot{\sigma}_{kl} \tag{14}$$

Furthermore, when the stress point moves outward along the brittle-ductile transition line, which is inclined at an angle of 60° to the horizontal-pressure axis in Fig. 1, the corresponding increments of the stress invariants are related by

$$d(J_2^{1/2}) = \sqrt{3}\frac{dI_1}{3} \tag{15}$$

Hence

$$\frac{S_{kl}\dot{\sigma}_{kl}}{2J_2^{1/2}} = \frac{1}{\sqrt{3}}\dot{\sigma}_{kk} \tag{16}$$

Substitution of (16) into (14) gives the inelastic strain rate during the brittle-ductile transition

$$D^I_{ij} = \frac{1}{h_t}\frac{S_{ij}S_{kl}}{4J_2}\dot{\sigma}_{kl} \tag{17}$$

This strain rate is purely deviatoric, with zero component of the volumetric strain rate. In (17), $h_t = dB/d\varphi = h/(1 - \sqrt{3}\mu)$.

CAP SURFACE

As discussed in the introduction, above the confining pressure p_t of the brittle-ductile transition, the Drucker-Prager yield criterion overestimates the yield stress in porous rocks, and inadequately predicts the volumetric strain response. DiMaggio and Sandler (1971) consequently developed a cap model by closing the Drucker-Prager yield cone with a cap, which crosses the hydrostatic stress axis and therefore allows compressive strain rates and yield under hydrostatic pressure. Although caps of various shapes (spherical, paraboloidal, and planar) were used in the literature, in this paper only an ellipsoidal cap will be considered. This cap has an equation

$$g = \frac{J_2}{B_2} + \frac{(I_1 - 3b)^2}{9A^2} - 1, \quad g = 0 \tag{18}$$

where A and B = two semiaxes of the ellipse shown in Fig. 1. If a stands for the hydrostatic compression state of stress, which is the horizontal apex of the ellipse, then $A = a - b$. The vertical apex of the ellipse is on the Drucker-Prager yield cone.

For any stress state on the cap, the associative flow rule will be assumed, i.e.

$$D^I_{ij} = \dot{\lambda}\frac{\partial g}{\partial \sigma_{ij}} \tag{19}$$

where $\dot{\lambda}$ = corresponding loading index. This, in view of (18), gives

$$D^I_{ij} = \dot{\lambda}\left(\frac{1}{B^2}S_{ij} + 2\frac{I_1 - 3b}{9A^2}\delta_{ij}\right) \tag{20}$$

The parameter b, which represents the hydrostatic pressure at the vertical apex of the ellipse, is related to B by (11). For the loading stress states on the cap, it is assumed that both b and B depend on the generalized inelastic strain φ, whose rate is

$$\dot{\varphi} = (2D^I_{ij}D^I_{ij})^{1/2} \tag{21}$$

When the stress state is at the intersection of the cap and the Drucker-Prager cone, i.e., at the vertical apex of the ellipse, (21) gives the same $\dot{\varphi}$ as (6), since along the brittle-ductile transition $\dot{\phi} = 0$.

The horizontal expansion of the cap during inelastic loading on the cap, i.e., the increase of the parameter a, is governed by inelastic volume strain ϑ, whose rate is

$$\dot{\vartheta} = D^I_{kk} \tag{22}$$

To obtain an expression for $a = a(\varphi)$, a relationship between pressure and volume change under pure compressive loading is needed. This has been studied by many, from both experimental and theoretical points of view, as discussed for porous rocks by Zhang et al. (1990). A simple expression, analogous to one originally suggested by DiMaggio and Sandler (1971), and later used by Resende and Martin (1985) and Simo et al. (1988), will here be adopted, such that

$$a(\vartheta) = a_0 - a_1 \ln(1 - \vartheta/\vartheta_{max}) \tag{23}$$

In (23), a_0 = pressure at which inelastic compaction begins; ϑ_{max} = maximum possible inelastic volume strain (related to the porosity of material); and a_1 = a fitting parameter (material constant).

Substituting (20) into (21) and (22), the rates of the inelastic strains $\dot{\varphi}$ and $\dot{\vartheta}$ can be expressed in terms of the loading index $\dot{\lambda}$ by

$$\dot{\varphi} = \eta_1\dot{\lambda}; \quad \dot{\vartheta} = \eta_2\dot{\lambda} \tag{24}$$

where

$$\eta_1 = 2\left[\frac{J_2}{B^4} + 2\frac{(I_1 - 3b)^2}{27A^4}\right]^{1/2}; \quad \eta_2 = 2\frac{I_1 - 3b}{3A^2} \tag{25}$$

The consistency condition $\dot{g} = 0$ provides the expression for $\dot{\lambda}$ in terms of the stress rate. After somewhat lengthy derivation, it follows that

$$\dot{\lambda} = \frac{1}{H}A_{ij}\dot{\sigma}_{ij} \tag{26}$$

In (26), the scalar parameter H is given by

$$H = 2\{B^3(I_1 - 3b)^2\psi_1 + [9A^3J_2 + \sqrt{3}AB^3(I_1 - 3b)]\psi_2\} \tag{27}$$

while the second-order tensor components are

$$A_{ij} = AB[9A^2S_{ij} + 2B^2(I_1 - 3b)\delta_{ij}] \tag{28}$$

The parameters ψ_1 and ψ_2, appearing in (27), are defined by

$$\psi_1 = \eta_2\frac{da}{d\vartheta} - \frac{1}{\sqrt{3}}\eta_1\frac{dB}{d\varphi}; \quad \psi_2 = \eta_1\frac{dB}{d\varphi} \tag{29}$$

Cross-Hardening between Cap and Cone

During inelastic loading with the stress state on the cap, the cap moves outward due to hardening and increase of the parameters a and B. Since the cap is attached to the Drucker-Prager cone, the cone also moves outward during loading on the cap. This is sketched in Fig. 2. On the other hand, during loading with the stress state on the cone, the cone moves outward isotropically, corresponding to increase of the parameter B. Since the introduced nonassociative flow rule of the second

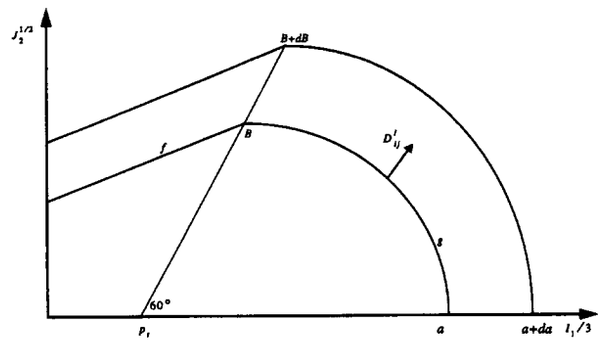

FIG. 2. Schematic Representation of Hardening Nature and Corresponding Yield Surface Expansion during Inelastic Loading on Cap

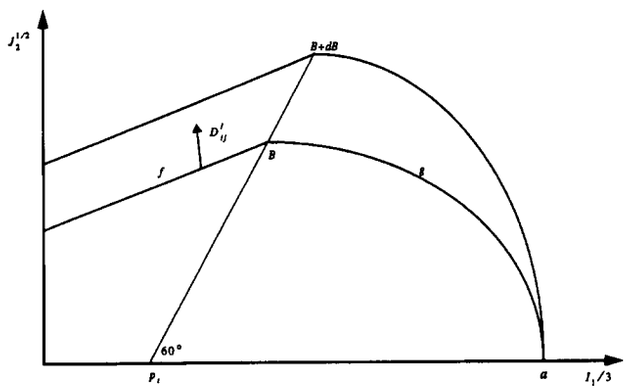

FIG. 3. Schematic Representation of Hardening Nature and Corresponding Yield Surface Expansion during Inelastic Loading on Cone

section predicts inelastic dilation during the loading on the cone, the definition of the rate $\dot{\vartheta}$, given in (22), is extended by stipulating that $\dot{\vartheta} = 0$ whenever the rate of inelastic volume strain is dilational (i.e., negative according to our convention of positive compressive strains). In this way, $\dot{a} = 0$ during inelastic loading on the cone. The resulting (cross) hardening of the cap, attached to the cone, is due to increase of the vertical semiaxis of the elliptical cap B, with the fixed horizontal apex of the cap. This is sketched in Fig. 3. Physically, the microcracks created during inelastic loading on the cone remain passive after unloading and subsequent pure hydrostatic loading along horizontal axis. Hence, without grain crushing and pore collapse created by loading on the cone, the parameter a remains constant and the horizontal apex of the cone does not move.

Loading along Brittle-Ductile Transition

During inelastic loading along the brittle-ductile transition line, i.e., when the stress point is at the corner between the Drucker-Prager cone and the ellipsoidal cap, one has $I_1 = 3b$ and $J_2^{1/2} = B$. Eqs. (27) and (28) reduce to

$$H = 36A^3Bh_t; \quad A_{ij} = 9A^3BS_{ij} \tag{30}$$

where, again, $h_t = dB/d\varphi$. Consequently, from (26) the loading index is

$$\dot{\lambda} = \frac{1}{4h_t} S_{ij}\mathring{\sigma}_{ij} \tag{31}$$

When this is substituted into (20), the inelastic strain rate during the brittle-ductile transition becomes exactly equal to that given by (17), and derived from the nonassociative flow rule and the Drucker-Prager yield condition. This is a consequence of the fact that the corner of the yield surface is always the point of the brittle-ductile transition, along which there is no inelastic volume strain rate. Hence, by using an elliptical cap that has a horizontal tangent at the corner, and the Prager-Drucker yield condition with a nonassociative inelastic potential whose gradient is perpendicular to the cap at the corner, the corresponding expressions for the inelastic strain rate are identical. In this way, the special treatment of the singular corner region, needed when employing the associative flow rules only (Resende and Martin 1985; Simo et al. 1988, etc.), is avoided. Note also that for the stress increments directed to the left of the brittle-ductile transition line and above the cone, the inelastic loading occurs on the cone. For the stress increments directed to the right of the brittle-ductile transition line and above the cap, the inelastic loading occurs on the cap.

If the stress point is at the horizontal apex of the elliptical cap, i.e., when $I_1 = 3a$ and $J_2^{1/2} = 0$, and if the loading is purely hydrostatic ($\mathring{\sigma}_{ij} = \dot{a}\delta_{ij}$), (27) and (28) reduce to

$$H = 36A^3B\frac{da}{d\vartheta}; \quad A_{ij} = 6A^2B^3S_{ij} \tag{32}$$

In this case the loading index is

$$\dot{\lambda} = \frac{A}{2}\dot{\vartheta} \tag{33}$$

The corresponding inelastic strain rate is

$$D^I_{ij} = \frac{1}{3}\dot{\vartheta}\delta_{ij} \tag{34}$$

Note that in the case of pressure-volume relationship given by (23), one has a hyperbolic type expression

$$\frac{da}{d\vartheta} = \frac{a_1}{\vartheta_{max} - \vartheta} \tag{35}$$

Also, from (24) and (33) it follows that the rate of the parameter φ, induced by the pure hydrostatic loading, is related to the rate of ϑ by $\dot{\varphi} = \sqrt{2/3}\dot{\vartheta}$.

FAILURE OR LIMITING SURFACE

The constitutive model of inelastic response is completed by introducing a fixed failure or limiting surface F, whose equation is

$$F = J_2^{1/2} - \alpha I_1 + k_1 \exp(-\beta I_1) - k_2, \quad F = 0 \tag{36}$$

where α, β, k_1, and k_2 = appropriate constants. The surface F has the following properties. It represents a failure surface for all stress states on F satisfying $J_2^{1/2} < B_*$, where B_* = ordinate of the intersection point with the brittle-ductile transition line. The failure occurs when the Drucker-Prager cone crosses the surface F, as sketched in Fig. 4. By failure, it is meant either the actual failure caused by unstable crack growth (at lower levels of confinement), or the onset of softening material response, with the localization of deformation into a shear band or fault (at moderate levels of confinement). The surface F further represents a limiting, ideally plastic yield surface for all stress states on F satisfying $J_2^{1/2} \geq B_*$. Hence, when the hardening cap crosses F, yielding at constant stress state occurs at the corner point. The same is true if the point on the limiting surface F is not a corner point, but a point reached by elastic unloading from the stress state on the expanded cap, as shown in Fig. 4. The ideally plastic yielding on the limiting surface is assumed to be governed by a nonassociative flow rule and the plastic potential

$$\hat{F} = J_2^{1/2} \tag{37}$$

The corresponding inelastic strain rate is

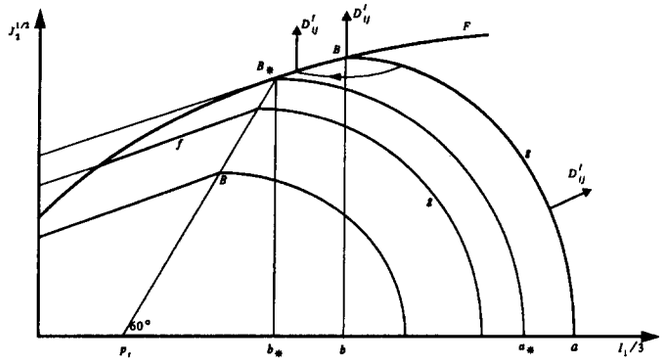

FIG. 4. Failure Occurring when Drucker-Prager Cone *f* Intersects Failure Surface *F*

$$D_{ij}^I = \dot{\rho}\,\frac{\partial \hat{F}}{\partial \sigma_{ij}} = \dot{\rho}\,\frac{S_{ij}}{2J_2^{1/2}} \tag{38}$$

In (38), $\dot{\rho}$ = a scalar multiplier, which is undetermined by the constitutive theory, but expressible in terms of the inelastic strain rate as $\dot{\rho} = (2D_{ij}^I D_{ij}^I)^{1/2}$. The structure of the plastic potential in (37) is selected so that the resulting inelastic strain rate, given by (38), is purely deviatoric. This is stipulated physically because the volumetric compaction, related to porosity of the material, is limited, and in the proposed model it occurs only during hardening of the cap, before the stress state reaches the surface F.

The hardening of the ellipsoidal cap, given by (18), is defined in the range $B \geq B_*$ in the following manner. The horizontal expansion of the cap, the function $a = a(\vartheta)$, is given by (23). The vertical expansion of the cap, i.e., the change of B, is such that the two semiaxes of the elliptical cap are related by

$$A = e(\vartheta)B \tag{39}$$

The ratio of the two ellipse axes $e = e(\vartheta)$ is determined according to experimental evidence. For example, DiMaggio and Sandler (1971) used a constant value of $e = 2.5$ for McCormick Ranch sand, while Simo et al. (1985) used the value $e = 4.43$ for concrete data. A nonconstant e was used by Sandler et al. (1976) to describe behavior of a partially saturated clay. Since $A = a - b$, and since from (36)

$$B = k_2 + 3\alpha b - k_1 \exp(-3\beta b) \tag{40}$$

substitution into (39) gives

$$a - b = e[k_2 + 3\alpha b - k_1 \exp(-3\beta b)] \tag{41}$$

For given functions $a = a(\vartheta)$ and $e = e(\vartheta)$, (41) can be numerically solved for $b = b(\vartheta)$. Substituting the result back into (40) gives $B(\vartheta)$. The function $A(\vartheta)$ can be obtained either from (39) or from $A(\vartheta) = a(\vartheta) - b(\vartheta)$. For example, if $k_1 = 0$, from (41) it follows that

$$b(\varphi) = \frac{a(\varphi) - k_2 e(\varphi)}{1 + 3\alpha e(\varphi)} \tag{42}$$

so that

$$A(\varphi) = \frac{e(\varphi)}{1 + 3\alpha e(\varphi)}\,[k_2 + 3\alpha a(\varphi)] \tag{43}$$

Inelastic loading on the cap above $B \geq B_*$ is governed by the associative flow rule, given by (20), with an appropriately determined expression for the loading index $\dot{\lambda}$. Indeed, in this case, the consistency condition, $\dot{g} = 0$, gives

$$9A^3BJ_2 + 2AB^3(I_1 - 3b)\dot{I}_1 = 18A^3J_2\dot{B} + 2B^3(I_1 - 3b)^2\dot{A} + 6AB^3(I_1 - 3b)\dot{b} \tag{44}$$

For the known dependence of A, B, and b on ϑ, the corresponding rates $\dot{A}$, $\dot{B}$, and $\dot{b}$ are easily expressed in terms of $\dot{\vartheta}$, and substitution into the consistency condition (44) gives the rate of the volumetric strain

$$\dot{\vartheta} = \frac{1}{H}\,A_{ij}\dot{\sigma}_{ij} \tag{45}$$

The parameter H is given by

$$H = 2\left[9A^3J_2\frac{dB}{d\vartheta} + B^3(I_1 - 3b)^2\frac{dA}{d\vartheta} + 3AB^3(I_1 - 3b)\frac{db}{d\vartheta}\right] \tag{46}$$

This parallels (27), which gives the parameter H for hardening of the cap in the range $B < B_*$. The second-order tensor components A_{ij} in (45) are the same as previously given by (28).

Since $\dot{\vartheta} = D_{kk}^I$, from (20) it follows that

$$\dot{\vartheta} = \dot{\lambda}\,\frac{2}{3}\,\frac{I_1 - 3b}{A^2} \tag{47}$$

At the corner, where the cap g meets the limiting surface F, $I_1 - 3b = 0$ and the volumetric strain rate becomes equal to zero. The expression for the loading index $\dot{\lambda}$ is now obtained from

$$\dot{\lambda} = \frac{3}{2}\,\frac{A^2}{I_1 - 3b}\,\dot{\vartheta} \tag{48}$$

with $\dot{\vartheta}$ determined by (45). Since $I_1 - 3b = 0$ and $\dot{\vartheta} = 0$ at the corner, $\dot{\lambda}$ becomes indeterminate there, as it should be since ideally plastic behavior prevails at the corner. Although both, $\dot{\lambda}$ and $\dot{\rho}$, are indeterminate at the corner points, they are easily related to each other at those points. Indeed, from (20) one has at the corner point

$$D_{ij}^I = \dot{\lambda}\,\frac{S_{ij}}{J_2} \tag{49}$$

Hence, comparison with (38) gives

$$\dot{\lambda} = \frac{1}{2}\,J_2^{1/2}\dot{\rho} \tag{50}$$

NUMERICAL RESULTS: TRIAXIAL COMPRESSION

In the triaxial compression test the specimen is subject to longitudinal compressive stress $\sigma_{33} = \sigma + p$, and a constant lateral confining pressure $\sigma_{11} = \sigma_{22} = p$. The difference between longitudinal and lateral stress σ is commonly referred to as the stress difference. The first stress invariant is $I_1 = \sigma + 3p$, while the second invariant of the deviatoric stress is $J_2 = \sigma^2/3$. From the Drucker-Prager yield condition, (1), it follows that

$$\frac{\sigma}{\sqrt{3}} = \frac{k + 3\mu p}{1 - \sqrt{3}\mu} \tag{51}$$

The rate of the monotonically increasing parameter φ is related to the stress rate $\dot{\sigma}$ by

$$\dot{\varphi} = \frac{1}{\sqrt{3}h_t}\,\dot{\sigma} \tag{52}$$

which follows from (8). In (52), $h_t = dB/d\varphi$. The longitudinal and volumetric inelastic strain rates are consequently

$$D_{33}^I = \frac{1}{\sqrt{3}h_t}\left(\frac{1}{\sqrt{3}} - \phi\right)\dot{\sigma} \tag{53}$$

$$D_{kk}^I = \frac{1}{\sqrt{3}h_t}\,(-3\phi)\dot{\sigma} \tag{54}$$

If p_t = brittle-ductile transition pressure, it readily follows that in triaxial compression under the confinement p

$$b(\varphi) - \frac{I_1}{3} = \frac{p_t - p}{1 - \sqrt{3}\mu} \tag{55}$$

Hence, in view of (12) and (13), the dilatancy parameter becomes

$$3\phi = \left(1 - \frac{p}{p_t}\right)^{n-1} 3\phi_0 \tag{56}$$

In the numerical evaluations of the model predictions it is taken that $n = 1/2$ and $\phi_0 = m_1(1 + m_2\varphi)$ for all φ. The function $B(\varphi)$ is conveniently selected as an inverse tangent function given by $B(\varphi) = c_0 \tan^{-1}(c_1 + c_2\varphi) - c_3$. According to experimental data for Salem limestone by Green (1992) shown in Figs. 5–7, the estimated value of 3μ is equal to 0.22. It is rather delicate to precisely estimate the value of the brittle-ductile transition pressure p_t, at which the longitudinal strain reaches a stage of an increase at constant stress difference σ, while the volumetric strain in that range of deformation remains approximately constant. The value of $p_t = 50$ MPa is accordingly selected. Initially, at $\varphi = 0$, the value of k is calculated to be 20.14 MPa. The values $m_1 = 0.075$ and $m_2 = 250$ are chosen to appropriately predict the inelastic volume

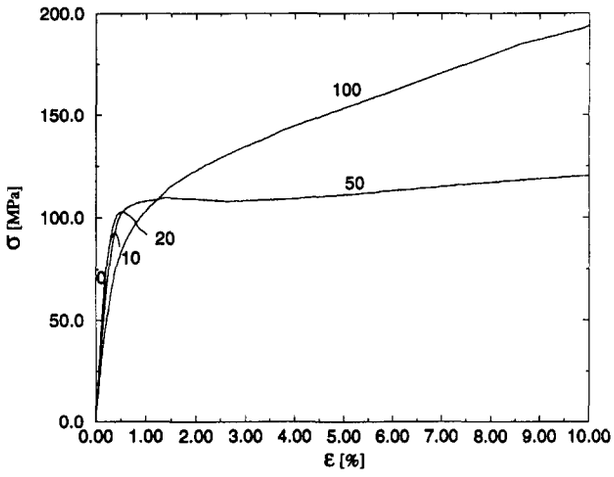

FIG. 5. Experimental Data (Green 1992) for Longitudinal Stress versus Longitudinal Strain during Triaxial Compression under Various Amounts of Confining Pressure (Indicated on Plots in MPa Units): Brittle-Ductile Transition Pressure is 50 MPa

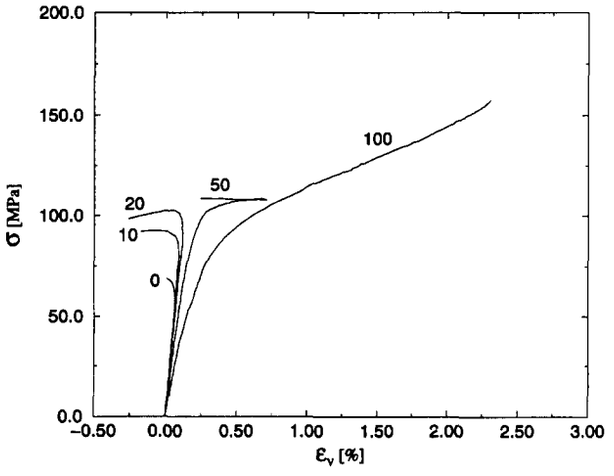

FIG. 6. Experimental Data (Green 1992) for Longitudinal Stress versus Volumetric Strain during Triaxial Compression under Various Amounts of Confining Pressure

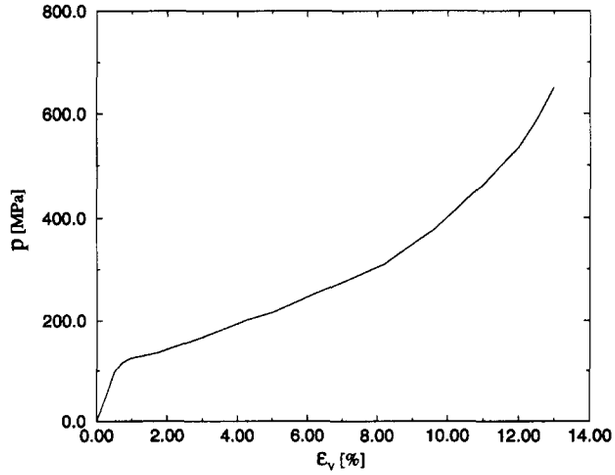

FIG. 7. Experimental Pressure-Engineering Volume Strain Relationship Obtained under Monotonic Purely Hydrostatic Compression (Green 1992)

dilatancy. The constants c_0 to c_3 appearing in the representation of the function $B(\varphi)$ are selected by a least-square fitting scheme using the symbolic manipulator Mathematica (Wolfram 1991), and their values are $c_0 = 525$ MPa, $c_1 = 12$, $c_2 = 3{,}000$, and $c_3 = 746$ MPa. The failure surface, represented by a single function that reproduces well the failure stress states in the whole range of the confining pressures, is more difficult to construct. As a first approximation, a linear functional form is assumed, with the coefficient $k_1 = 0$ in (36). The remaining constants are appropriately chosen to be $\alpha = 0.159$ and $k_2 = 28.45$ MPa. It is found that the cap first reaches the failure surface at the value of the hardening parameter $\varphi_* = 0.02$.

The initial Young's modulus of the Salem limestone is about $E = 37.5$ GPa, while the Poisson ratio is about $\nu = 0.22$. These values change as deformation proceeds, particularly at lower confining pressures. For example, according to experimental data at the confining pressure of 30 MPa, E decreases by an amount of about 15% from the inception of inelastic deformation to conditions near failure. This can be implemented in the calculations. For example, Xiang et al. (1991) used variable elastic constants in their study of high porosity Berea sandstone, and assumed that elastic bulk modulus depends on the total volumetric strain, while shear modulus was assumed to depend on the confining pressure. Sandler et al. (1976) used a hypoelastic type model with somewhat more involved expressions for the variable shear and bulk moduli. However, to better illustrate the features of the inelastic constitutive model proposed in this paper, the results given in this section are obtained by using the constant values of E and ν, equal to their initial values before any damage took place.

Fig. 8 shows the longitudinal and volumetric strain responses obtained at different values of the confining pressure. The strains are measured relative to hydrostatically compressed initial configuration. The curves corresponding to pressures $p_1 = 20$ MPa and $p_2 = 35$ MPa terminate due to brittle failure that occurs when the Drucker-Prager cone crosses the failure surface at the respective failure stress levels. The curve corresponding to pressure $p_t = 50$ MPa is associated with the brittle-ductile transition. A perfectly plastic response and unlimited longitudinal strain occur at the limiting stress state. The volumetric strain response is linear due to absence of inelastic volume strain at the brittle-ductile transition. Below the brittle-ductile transition, i.e., in the confining pressure range $p < p_t$, the inelastic dilation occurs and the net volumetric strain gradually changes from compressive to tensile, in agreement with experimental observations (Fig. 6). The dilatancy factor ϕ increases from the inception of inelastic de-

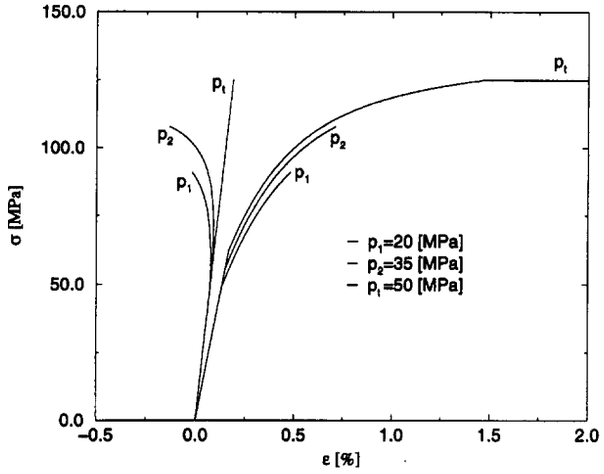

FIG. 8. Longitudinal Stress versus Longitudinal Strain (Left Three Plots) and Longitudinal Stress versus Volumetric Strain (Right Three Plots) at Different Values of Confining Pressure

formation to conditions near failure. For example, at the confining pressure of 20 MPa it increases by approximately a factor of two, from 0.058 to 0.13. At the transition confining pressure p_t, $\phi = 0$ throughout the whole deformation range.

In the triaxial compression above the brittle-ductile transition, the loading index is given by (26), in which

$$A_{ij}\delta_{ij} = AB[6A^2\sigma + 2B^2(I_1 - 3b)]\dot{\sigma} \tag{57}$$

The parameter H appearing in (26) is defined by (27), providing that the hardening is in the range before the cap reached the failure surface. In the triaxial compression, furthermore

$$I_1 - 3b = \sigma + 3(p - p_t) - B/\sqrt{3} \tag{58}$$

The corresponding longitudinal and volumetric inelastic strain rates are

$$D^I_{33} = \frac{2}{3}\left(\frac{\sigma}{B^2} + \frac{I_1 - 3b}{3A^2}\right)\dot{\lambda} \tag{59}$$

$$D^I_{kk} = \frac{2}{3}\frac{I_1 - 3b}{A^2}\dot{\lambda} \tag{60}$$

In the range of hardening when the apex of the cap is on the failure surface, the loading index $\dot{\lambda}$ is given by (48). The rate $\dot{\vartheta}$ is calculated from (45), with the hardening parameter H determined by (46). The trace product $A_{ij}\delta_{ij}$ is again given by (57).

As discussed in the third section, the horizontal expansion of the cap is governed by the function $a(\vartheta)$, given by (23). The corresponding constants appearing in this function are determined in accordance with available pressure-volume data for Salem limestone (Fig. 7), and have the values: $a_0 = 120$ MPa, $a_1 = 350$ MPa, and $\vartheta_{max} = 0.15$. Recall that a_0 = pressure at which the inelastic compaction begins, while ϑ_{max} = maximum possible inelastic volume strain, assumed to be approximately equal to the porosity of considered limestone, which is about 15%.

The function $e(\vartheta)$ appearing in (39) is assumed to be a linear function of ϑ. If A_* (which is equal to $a_* - b_*$ in Fig. 4) and B_* denote the two semiaxes of the elliptical cap at the instance when the cap first reaches the failure surface (which occurs at the ϑ_* value of ϑ), the corresponding ratio is $e_* = A_*/B_*$. During further expansion of the cap this ratio is assumed to change according to $e = e_* + e_1(\vartheta - \vartheta_*)$, where e_1 = a constant. The magnitude of this constant influences the hardening rate, and the volumetric compressibility. In the performed calculations, the value $e_1 = 10$ was used. The values e_* and ϑ_* depend on the confining pressure p. For example, if $p = p_t$, it is found that $e_* = 0.4$, while $\vartheta_* = 0$ due to absence of inelastic volume change along the brittle-ductile transition. In the case of pure hydrostatic loading, $\vartheta_* = \sqrt{3/2}\varphi_* = 0.0245$, since $\varphi_* = 0.02$. The value of a_* corresponding to ϑ_* is obtained from (23), which gives $a_* = 182.4$ MPa. Since $B_* = 125/\sqrt{3}$ MPa and $b_* = p_t + B_*/\sqrt{3} = 91.7$ MPa, it follows that $A_* = a_* - b_* = 90.75$ MPa. Therefore, in this case the semiaxes ratio is $e_* = A_*/B_* = 1.26$.

Fig. 9 gives the stress–longitudinal strain response at various confining pressures. The curve corresponding to $p = p_t$ is the stress-strain response at the brittle-ductile transition, while the curve corresponding to $p = p_2$ is the stress-strain response in the brittle range of deformation, below the brittle-ductile transition, as shown previously in Fig. 8. The remaining three curves are associated with the confining pressures $p > p_t$, and represent the stress-strain responses above the brittle-ductile transition. The increased confining pressure clearly extends the hardening range of the material response. It also decreases the stress threshold at which inelastic deformation occurs, both in agreement with experimental observations, as shown in Fig. 5. A slight discontinuity in slope of the stress-strain curves occurs at the instant when the vertical apex of the cap first reaches the failure surface. This is because the subsequent motion of the cap and the corresponding hardening rule are defined differently from those in the range of deformation before the cap first reaches the failure surface. This discontinuity, as

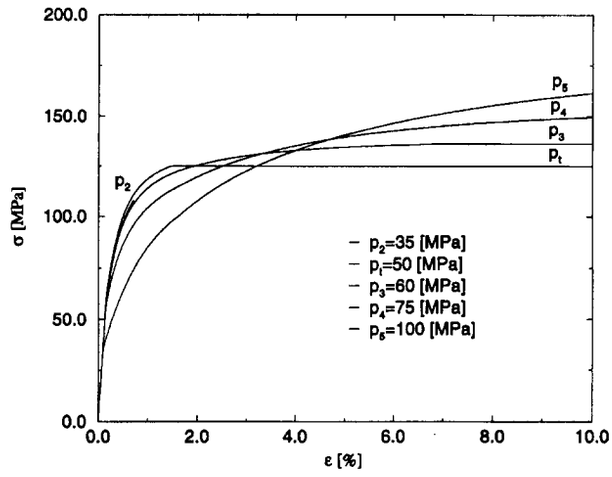

FIG. 9. Longitudinal Stress versus Longitudinal Strain at Various Confining Pressures

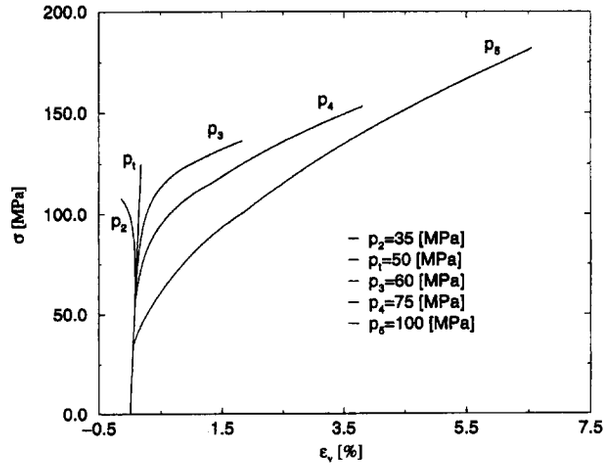

FIG. 10. Longitudinal Stress versus Volumetric Strain Response at Five Representative Values of Confining Pressure

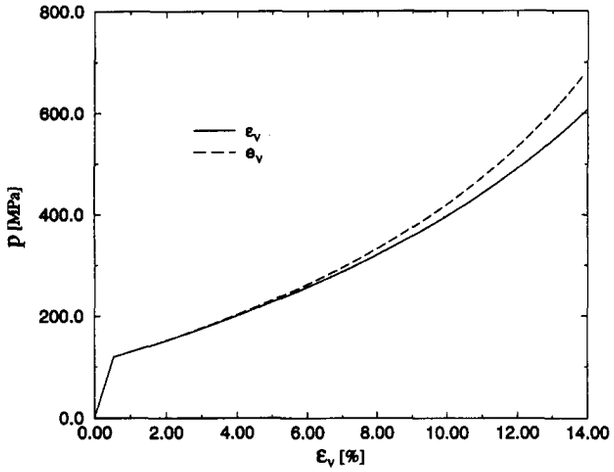

FIG. 11. Predicted Pressure versus Volume Strain Relationship under Pure Hydrostatic Compression Loading [Curves Corresponding to Logarithmic (ε_v) and Engineering (e_v) Measures are Shown]

TABLE 1. Material Parameters of Model

Parameters (1)	Values (2)
p_t	50 MPa
c_0	525 MPa
c_1	12
c_2	3,000
c_3	746 MPa
μ	0.073
m_1	0.075
m_2	250
n	1/2
k_2	28.45 MPa
α	0.159
a_0	120 MPa
a_1	350 MPa
ϑ_{max}	0.15
e_1	10
E	37.5 GPa
ν	0.22

well as the hardening slopes of the stress-strain curves, can be controlled by the appropriate selection of the function $e(\vartheta)$.

Fig. 10 is the stress–volumetric strain response at the five representative values of the confining pressure. Below the brittle-ductile transition the inelastic volume dilation soon overcome elastic compressibility of the material, leading to the overall tensile volume strain. Above the brittle-ductile transition the inelastic volume strains are compressive. The maximum volumetric strain that can be achieved increases with the increase of confining pressure. The corresponding numerical values for a given material are again conveniently adjusted by the form of the function $e(\vartheta)$. The calculated pressure-volumetric strain behavior in the case of pure hydrostatic loading is shown in Fig. 11. The curves corresponding to the logarithmic and engineering measures of the volumetric strain are both shown.

Summary of Material Parameters

The material parameters of a proposed constitutive model and their numerical values for the Salem limestone are summarized in Table 1.

CONCLUSIONS

The pressure-dependent constitutive model proposed in this paper is capable of describing the brittle-ductile transition in porous rocks and similar materials. Below the brittle-ductile transition, it predicts the brittle stress-strain response, with inelastic volume dilation. Above the brittle-ductile transition, the increased ductility and hardening rates prevail, with the overall inelastic volume compressibility. Along the brittle-ductile transition the inelastic volume change does not occur. The model combines the associative and nonassociative flow rules, in conjunction with the Drucker-Prager hardening cone, an ellipsoidal cap, and a failure surface. The model is sufficiently simple, and easily implemented in numerical evaluations. A special treatment of the singular corner region at the intersection of the cap and failure surface, required in other suggested models, is eliminated by a nonassociative structure of the introduced flow rules. The material constants that appear in the model are related to specific physical aspects of the material response, and are easy to determine without using an elaborate optimization scheme. The worthy tasks for further research are the representation of the progressive degradation of elastic material properties and the development of induced elastic anisotropy, with their relationship to the structure of inelastic constitutive equations.

ACKNOWLEDGMENTS

The writers are grateful for the support provided by the research contract with the Waterways Experiment Station (WES), U.S. Army Corps of Engineers. Conversations with Dr. J. Zelasko of WES are kindly acknowledged.

APPENDIX. REFERENCES

Ashby, M. F., and Sammis, C. G. (1990). "The damage mechanics of brittle solids in compression." *Pure and Applied Geophys.*, 133(3), 489–521.

Bathe, K. J., Snyder, M. D., Cimento, A. P., and Rolph, W. D. (1980). "On some current procedures and difficulties in finite element analysis of elastic-plastic response." *Comp. and Struct.*, 12, 607–624.

Bažant, Z. P., and Kim, S. S. (1979). "Plastic-fracturing theory for concrete." *J. Engrg. Mech.*, ASCE, 105(3), 407–428.

Bresler, B., and Pister, K. S. (1958). "Strength of concrete under combined stresses." *ACI J.*, 30(3), 321–345.

Chandler, H. W. (1985). "A plasticity theory without Drucker's postulate, suitable for granular materials." *J. Mech. and Phys. of Solids*, 33(3), 215–226.

Chen, W. F., and Han, D. J. (1988). *Plasticity for structural engineers.* Springer-Verlag, New York, N.Y.

Desai, C. S. (1980). "A general basis for yield, failure and potential functions in plasticity." *Int. J. Numer. and Analytical Methods in Geomech.*, 4, 361–375.

Desai, C. S., and Siriwandane, H. J. (1984). *Constitutive laws for engineering materials.* Prentice-Hall, Englewood Cliffs, N.J.

Desai, C. S., Somasundaram, S., and Frantziskonis, G. (1986). "A hierarchical approach for constitutive modeling of geologic materials." *Int. J. Numer. and Analytical Methods in Geomech.*, 10(3), 225–257.

Desai, C. S., and Varadarajan, A. (1987). "A constitutive model for quasi-static behavior of rock salt." *J. Geophys. Research*, 92(B11), 11,445–11,456.

DiMaggio, F. L., and Sandler, I. S. (1971). "Material model for granular soils." *J. Engrg. Mech.*, ASCE, 97(3), 935–950.

Dougill, Y. W. (1975). "Some remarks on path independence in the small in plasticity." *Quarterly of Appl. Math.*, 33, 233–243.

Dougill, Y. W. (1983). "Path dependence and a general theory for the progressively fracturing solid." *Proc., Royal Soc.*, London, England, A 390, 341–351.

Dougill, Y. W., and Rida, M. A. M. (1980). "Further consideration of progressively fracturing solids." *J. Engrg. Mech.*, ASCE, 106(5), 1021–1038.

Dragon, A., and Mróz, Z. (1979). "A continuum model for plastic brittle behavior of rock and concrete." *Int. J. Engrg. Sci.*, 17, 121–137.

Drucker, D. C., Gibson, R. E., and Hankel, D. J. (1957). "Soil mechanics and work-hardening theories of plasticity." *Trans.*, ASCE, 122, 338–346.

Drucker, D. C., and Prager, W. (1952). "Soil mechanics and plastic analysis or limit design." *Quarterly of Appl. Math.*, 10, 157–175.

Evans, B., Fredrich, J. T., and Wong, T.-F. (1990). "The brittle-ductile transition in rocks: Recent experimental and theoretical progress." *The*

brittle-ductile transition in rocks, The Heard Volume, Geophys. Monograph Ser., Vol. 56, A. G. Duba et al., eds., Am. Geophys. Union (AGU), Washington, D.C., 1–20.
Frantziskonis, G., Desai, C. S., and Somasundaram, S. (1986). "Constitutive model for nonassociative behavior." *J. Engrg. Mech.*, ASCE, 112(9), 932–946.
Fredrich, J. T., Evans, B., and Wong, T.-S. (1989). "Micromechanics of the brittle to plastic transition in Carrara marble." *J. Geophys. Res.*, 94(B4), 4129–4145.
Green, M. L. (1992). *Laboratory tests on Salem limestone*. Geomechanics Div., Struct. Lab., Dept. of the Army, Vicksburg, Miss.
Han, D. J., and Chen, W. F. (1985). "A uniform hardening plasticity model for concrete materials." *Mech. of Materials*, 4, 283–302.
Hegemier, G. A., and Reed, H. E. (1985). "On deformation and failure of brittle solids: some outstanding issues." *Mech. of Materials*, 4, 215–260.
Hirth, G., and Tullis, J. (1989). "The effects of pressure and porosity on the micromechanics of the brittle-ductile transition in quartzite." *J. Geophys. Res.*, 94(B12), 17,825–17,838.
Horii, H., and Nemat-Nasser, S. (1986). "Brittle failure in compression: splitting, faulting and brittle-ductile transition." *Phil. Trans., Royal Soc.*, London, England, A 319, 337–374.
Jaeger, J. C., and Cook, N. G. W. (1976). *Fundamentals of rock mechanics*. Chapman and Hall, London, England.
Ju, J. W. (1989). "On energy based coupled elastoplastic damage theories: constitutive modeling and computational aspects." *Int. J. Solids and Struct.*, 25(7), 803–833.
Kim, M. K., and Lade, P. V. (1984). "Modeling rock strength in three dimensions." *Int. J. Rock Mech. Min. Sci. Geomech. Abstr.*, 31, 21–33.
Kranz, R. L. (1983). "Microcracks in rocks: A review." *Tectonophysics*, 100, 449–480.
Lade, P. V. (1977). "Elasto-plastic stress-strain theory for cohesionless soil with curved yield surfaces." *Int. J. Solids and Struct.*, 13, 1019–1035.
Lade, P. V., and Duncan, J. M. (1975). "Elastoplastic stress-strain theory for cohesionless soil." *J. Geotech. Engrg.*, ASCE, 101(10), 1037–1053.
Lubarda, V. A. (1994). "An analysis of large-strain damage elastoplasticity." *Int. J. Solids and Struct.*, 31(21), 2951–2964.
Lubarda, V. A., and Krajcinovic, D. (1995a). "Constitutive structure of the rate theory of damage in brittle elastic solids." *Appl. Math. Comp.*, 67, 81–101.
Lubarda, V. A., and Krajcinovic, D. (1995b). "Some fundamental issues in the rate theory of damage-elastoplasticity." *Int. J. Plasticity*, 11(7), 763–797.
Lubarda, V. A., Krajcinovic, D., and Mastilovic, S. (1995). "Rate theory of damage in elastic solids with unequal tensile and compressive strengths." *Engrg. Fracture Mech.*, 49(5), 681–697.
Lubarda, V. A., Mastilovic, S., and Knap, J. (1996). "Some comments on plasticity postulates and non-associative flow rules." *Int. J. Mech. Sci.*, 38(3), 247–258.
Nemat-Nasser, S. (1983). "On finite plastic flow of crystalline solids and geomaterials." *J. Appl. Mech.*, 50, 1114–1126.
Nemat-Nasser, S., and Hori, M. (1993). *Micromechanics—overall properties of heterogeneous solids*. North-Holland, Amsterdam, The Netherlands.
Nemat-Nasser, S., and Shokooh, A. (1980). "On finite plastic flows of compressible materials with internal friction." *Int. J. Solids and Struct.*, 16(6), 495–514.
Ortiz, M. (1985). "A constitutive theory for the inelastic behavior of concrete." *Mech. of Materials*, 4, 67–93.
Paterson, M. S. (1978). *Experimental rock deformation—The brittle field*, Springer-Verlag, New York, N.Y.
Prevost, J. H., and Höeg, K. (1975). "Effective stress-strain-strength model for soils." *J. Geotech. Engrg.*, ASCE, 101(3), 259–278.
Read, H. E., and Hegemier, G. A. (1984). "Strain softening of rock, soil and concrete—a review article." *Mech. of Materials*, 3, 271–294.
Resende, L., and Martin, J. B. (1985). "Formulation of Drucker-Prager cap model." *J. Engrg. Mech.*, ASCE, 111(7), 855–881.
Rudnicki, J. W., and Rice, J. R. (1975). "Conditions for localization of deformation in pressure-sensitive dilatant materials." *J. Mech. and Phys. Solids*, 23, 371–394.
Rutter, E. H., and Hadizadeh, J. (1991). "On the influence of porosity on the low-temperature brittle-ductile transition in siliciclastic rocks." *J. Struct. Geol.*, 13, 609–614.
Sammis, C. G., and Ashby, M. F. (1986). "The failure of brittle porous solids under compressive stress states." *Acta Metall.*, 34(3), 511–526.
Sandler, I. S., DiMaggio, F. L., and Baladi, G. Y. (1976). "Generalized cap model for geological materials." *J. Geotech. Engrg.*, ASCE, 102(7), 638–699.
Sandler, I. S., and Rubin, D. (1979). "An algorithm and a modular subroutine for the cap model." *Int. J. Numer. and Analytical Methods in Geomech.*, 3. 173–186.
Senseny, P. E., Fossum, A. F., and Pfeifle, T. W. (1983). "Non-associative constitutive laws for low porosity rocks." *Int. J. Numer. and Analytical Methods in Geomech.*, 7, 101–115.
Simo, J. C., and Ju, J. W. (1987). "Strain- and stress-based continuum damage models—I. Formulation." *Int. J. Solids and Struct.*, 23(7), 821–840.
Simo, J. C., Ju, J. W., Pister, K. S., and Taylor, R. L. (1987). "Assessment of cap model: consistent return algorithms and rate-dependent extension." *J. Engrg. Mech.*, ASCE, 114(2), 191–218.
Wolfram, S. (1991). *Mathematica—A system for doing mathematics by computer*. Addison-Wesley, New York, N.Y.
Wong, T.-F. (1990). "Mechanical compaction and the brittle-ductile transition in porous sandstones." *Deformation mechanisms, rheology and tectonics*, R. J. Knipe and E. H. Rutter, eds., Spec. Publ. No. 54, Geological Soc., London, England, 111–122.
Wong, T.-F., Szeto, H., and Zhang, J. (1992). "Effect of loading path and porosity on the failure mode of porous rocks." *Appl. Mech. Rev.*, 45, 281–293.
Xiang, Y., Huang, S., and Khan, A. S. (1991). "Elastic-plastic behavior of high porosity rock." *Anisotropy and localization of plastic deformation*, J.-P. Boehler and A. S. Khan, eds., Elsevier Applied Science, New York, N.Y., 270–273.
Yazdani, S., and Schreyer, H. L. (1989). "Combined plasticity and damage mechanics model for plane concrete." *J. Engrg. Mech.*, 116(7), 1435–1450.
Zaman, M. M., Desai, C. S., and Faruque, M. O. (1982). "An algorithm for determining parameters for cap model from raw laboratory test data." *Proc., 4th Int. Conf. Numer. Methods in Geomech.*, B. Eisenstein, ed., Vol. 1, A. A. Balkema, Rotterdam, The Netherlands, 275–285.
Zhang, J., Wong, T.-F., and Davis, D. M. (1989). "The brittle to ductile transition in porous sandstones." *Trans., Am. Geophysical Union*, 70, 1360–1368.
Zhang, J., Wong, T.-F., and Davis, D. M. (1990). "Micromechanics of pressure-induced grain crushing in porous rocks." *J. Geophys. Res.*, 95(B1), 341–352.
Zheng, Z., McLennan, J., and Martin, W. (1991). "Compressive stress-induced microcracks and effective elastic properties of limestone and concrete." *Final Tech. Rep., Submitted to AFOSR/XOT*, Terra Tek, Inc., Salt Lake City, Utah.